Manuscript prepared for Atmos. Chem. Phys. Discuss.
with version 1.21 of the LaTeX class copernicus.cls.
Date: 20 July 2010

Supplemental Information for Oxidative capacity of the Mexico City atmosphere - Part 2: A RO_x radical cycling perspective

P.M. Sheehy[1,2], **R. Volkamer**[1,3,4], **L.T. Molina**[1,2], **and M.J. Molina**[1,3]

[1]Massachusetts Institute of Technology, Cambridge MA
[2]Molina Center for Energy & the Environment, La Jolla CA
[3]University of California at San Diego, La Jolla CA
[4]University of Colorado at Boulder and CIRES, Boulder CO

Correspondence to: P. Sheehy and R. Volkamer
(sheehy@alum.mit.edu and rainer.volkamer@colorado.edu)

1 Model Constraints

1.1 Alkanes

Alkanes were scaled using a combination of data collected via whole air canister sampling (Velasco et al., 2007) and continuous FTIR measurements (Table 1). For the days that both measurements from canister sampling and FTIR sampling are available, the data show good agreement. The concentration of each individual alkane species, relative to the sum of the alkane species (in ppbC), is effectively constant throughout the day. Diurnal profiles for each alkane species were subsequently determined by scaling continuous FTIR measurements (of effective C-H stretches) by the ratios determined from canister speciation. Based on measurement uncertainty from the GC-FID and FTIR, and the scaling methodology, we estimate uncertainty for the alkanes input as $\pm 25\%$.

1.2 Alkenes

The concentrations of alkene species (Table 1) were determined using the canister data and measurements from a Fast Isoprene Sensor (FIS). A generic FIS signal was plotted against the alkene data from the canister samples accounting for the response of the FIS towards different olefin species (Velasco et al., 2007); for species in which the response factor was not available, the response factor is assumed to be unity. The scaling factors derived from the canister data are used with the continuous FIS data to generate time-resolved input parameters for the alkenes. The scaling factors for alkenes included in the box model that were not directly measured are determined using speciation profiles, as found in the literature (Harley et al., 1992). We estimate uncertainty for the alkenes input as $\pm 25\%$.

1.3 Aromatics

The concentrations of aromatic species in the model are determined by direct DOAS measurements (Volkamer et al., 2004, 2005) following evaluation protocols developed by Volkamer et al. (1998), a scaling methodology using canister data, and emissions factors (Harley et al., 1992).

The compounds measured directly by DOAS and scaled using other measurements are listed in Table 1. The direct measurement of benzene is used in conjunction with canister data to scale aromatic compounds not measured by DOAS. The DOAS instruments also measured a general mono-substituted benzene signal, which is assumed to be a weighted response from ethyl benzene, n-propyl benzene, and i-propyl benzene (Axelsson et al., 1995). The compounds directly measured by DOAS, with measurement uncertainties include: toluene ($\pm$15%), benzene ($\pm$15%), o-xylene ($\pm$15%), m-xylene ($\pm$15%), p-xylene ($\pm$15%), styrene ($\pm$15%), benzaldehyde ($\pm$15%). The compounds scaled via canister speciation have estimated uncertainties of ($\pm$25%).

1.4 Oxygenated VOC

In addition to the alkanes, alkenes, and aromatic species, a number of alcohols, aldehydes, ketones, esters, ethers, and organic acids were constrained in the model, see Table 1 for the list of species and scaling methodology. Most notably, formaldehyde (HCHO) and glyoxal were measured by DOAS, both with an uncertainty of $\pm$25%. Based on the scaling methodology employed here, we estimate that the uncertainty for the oxygenated compounds not directly measured is $\pm$50%.

Note that for the oxygenated compounds not directly measured, aerosol related loss processes - as discussed for glyoxal in Volkamer et al. (2006), for example - are not included.

2 Chain length

For the sake of reference, we have provided all the chain length parameters - both n(OH) and ω - for each modeled scenario in Figure 1.

Table 1. VOC constraints used for box modeling based on measurements from MCMA-2003. The input for each species is determined by either i) continuous measurement, ii) scaling to a continuous measurement via speciation as determined by co-located canister sampling, or iii) scaled to a continuous measurement via emission factors taken from Harley et al. (1992) and EPA (2004).

alkanes		**alkenes**		**aromatics**		**oxygenates (ctd)**	
species	SF x10^{-2}	species	SF x10^{-2}	species	SF x10^{-2}	species	SF x10^{-2}
methane	FTIR	ethene	80 ^{C}	benzene	DOAS	methanol	PTRMS
ethane	2.18 ^{A}	propene	44 ^{C}	toluene	DOAS	ethanol	15 ^{H}
propane	42.6 ^{A}	2-methylpropene	31 ^{C}	m-xylene	DOAS	1-propanol,2-propanol	5
i-butane	7.40 ^{A}	c-2-butene	4.5 ^{C}	p-xylene	DOAS	1-butanol,2-butanol	2 ^{H}
n-butane	19.7 ^{A}	t-2-butene	5.0 ^{C}	styrene	DOAS	2-methyl-1(2)-propanol	2 ^{H}
i-pentane	8.37 ^{A}	1-pentene	5.9 ^{C}	benzaldehyde	DOAS	ethylene glycol	25 ^{H}
n-pentane	3.69 ^{A}	c-2-pentene	2.8 ^{C}	ethyl benzene	62 ^{F}	propylene glycol	10 ^{H}
n-hexane	1.98 ^{A}	t-2-pentene	5.0 ^{C}	n-propyl benzene	16 ^{F}	2-methoxy ethanol	2 ^{H}
2-methylpentane	2.77 ^{A}	2-methyl-1-butene	12 ^{C}	i-propyl benzene	22 ^{F}	2-ethoxy ethanol	2 ^{H}
3-methylpentane	1.95 ^{A}	2-methyl-2-butene	8.5 ^{C}	o-xylene	53 ^{E}	1-methoxy 2-propanol	2 ^{H}
2,2-dimethylbutane	0.97 ^{A}	1,3-butadiene	4.8 ^{C}	1,2,4-trimethylbenzene	55 ^{E}	2-butoxy ethanol	2 ^{H}
2,3-dimethylbutane	0.64 ^{A}	isoprene	3.9 ^{C}	1,3,5-trimethylbenzene	19 ^{E}	1-butoxy 2-propanol	2 ^{H}
n-heptane	0.64 ^{A}	1-butene	15 ^{D}	1,2,3-trimethylbenzene	14 ^{E}	acetone	PTRMS
2-methylhexane	0.80 ^{A}	3-methyl-1-butene	5.9 ^{D}	o-ethyl toluene	14 ^{E}	methyl ethyl ketone	PTRMS
3-methylhexane	1.10 ^{A}	1-hexene	2.1 ^{D}	p-ethyl toluene	30 ^{E}	acetic acid	PTRMS
n-octane	0.26 ^{A}	c-2-hexene	2.1 ^{D}	m-ethyl toluene	14 ^{E}	methyl i-butyl ketone	13 ^{I}
n-nonane	0.22 ^{A}	t-2-hexene	3.8 ^{D}	**oxygenates**		ethyl acetate	0.6 ^{E}
n-decane	0.27 ^{A}	2,3-dimethyl-2-butene	2.1 ^{D}	formaldehyde (HCHO)	DOAS	n-propyl + i-propyl acetate	0.15 ^{E}
cyclohexane	0.31 ^{A}	acetylene	1.9 ^{E}	acetaldehyde	PTRMS	n-butyl acetate	0.21 ^{E}
n-undecane	1.6 ^{B}			propanal	4.5 ^{G}	methyl t-butyl ether	1.1 ^{E}
n-dodecane	0.32 ^{B}						

A-scaled to FTIR(C−H) based on canister speciation
B-scaled to FTIR(C−H) based on emission factors
C-continuous FOS signal scaled based on canister speciation
D-scaled to FOS signal based on emissions factors
E-scaled to DOAS-benzene based on canister speciation
F-scaled to mono-substituted benzene DOAS profile based on canister speciation
G-scaled to DOAS-$HCHO$ based on emissions factors
H-scaled to PTRMS-CH_3OH based on emission factors
I-scaled to PTRMS-MEK based on emission factors

3 OH production and loss: Measurement imbalance

The hydroxyl radical is a short-lived species in the atmosphere, and is in steady-state on a time scale of 0.1 s. Shirley et al. (2006) note the balance observed in median OH production, P(OH), and OH loss, L(OH). The only notable exception is between 07:00-08:00 when OH production

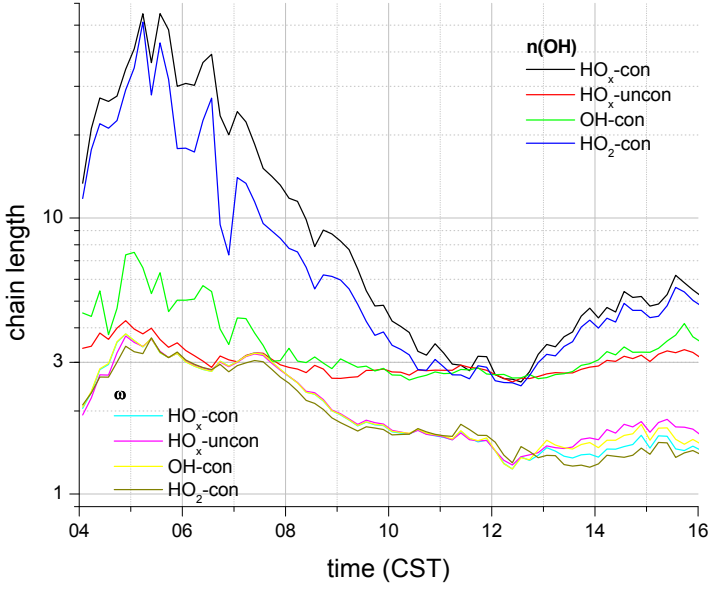

Fig. 1. Both chain length parameters are shown for each scenario (see Section 2). Note the differences in the n(OH) values for each scenario compared to the consistent overlap for the ω values throughout the day.

is twice OH loss. P(OH) and L(OH) are defined here as:

$$\mathrm{P(OH)} = k_{\mathrm{HO_2+NO}}[\mathrm{HO_2}][\mathrm{NO}] + \mathrm{OH_{new}}, \text{and} \tag{1}$$

$$\mathrm{L(OH)} = k_{\mathrm{OH+NO_x}}[\mathrm{OH}][\mathrm{NO_x}] + k_{\mathrm{OH+VOC}}[\mathrm{OH}][\mathrm{VOC}]. \tag{2}$$

The production of OH via reaction between HO_2 and NO accounts on average for more than 80% of P(OH). OH_{new} is equivalent to initiation i.e., the generation of a OH radical from the breakdown of a closed shell species e.g., O_3, and is discussed in more detail elsewhere (Volkamer et al., 2010). The extensive suite of data, including HO_x and OH loss measurements, provides the means to calculate both OH production and loss throughout the campaign, as shown in Figure 2-A. The difference between median P(OH) and L(OH), $L(OH)_{med}-P(OH)_{med}$, is shown with a 2σ *experimental* uncertainty, which is duplicated from the work by Shirley et al. (2006). We have also included the median difference between individual measurements, $(L(OH)_{ind}-P(OH)_{ind})_{med}$, and plotted it with 1σ standard deviation i.e., the statistical scatter of the difference between production and loss on an individual basis. Even though the L−P difference plots are similar, the blue error bars emphasize the considerable scatter of individual measurements, and reflect what we consider an imbalance in the measurements. In other words, the "balance" between median production and median loss observed by Shirley et al. (2006) is a function of averaging large statistical scatter, rather than a balanced set of measurements bound by experimental certainty.

To illustrate this more clearly, the difference between OH production and loss from individual measurements as a function of NO is shown in Figure 2-B. The difference is shown as the absolute value of [P(OH)−L(OH)]/P(OH), and values are further separated by 1) P(OH) > L(OH), and 2) P(OH) < L(OH). The 2σ experimental uncertainty is taken as 55% (Shirley et al., 2006), and represented as a dotted line in the figure. Any point *below* this line represents a balance between production and loss within experimental uncertainty, whereas any point *above* the line represents an imbalance in the measurements. By this estimate, 55% of the individual measurements fall outside of the experimental uncertainty – rather than the expected 33% based on a 2σ confidence level – 75% of which are at values of NO lower than 10 ppb (i.e., when confidence in the measurements is highest).

We are not challenging the accuracy of the HO_x concentration or OH loss measurements, which are of the highest quality attainable to date. The noted imbalance is also independent of the HO_x calibration. The lack of agreement between OH production and OH loss has drastic implications for any box model. Our MCM box model is simply unable to predict the observed

HO_2 concentrations because of high concentrations of NO_x in the same air mass. Notably, we use measurements taken at *similar* heights. Although unlikely, the imbalance in the measurements may be the result of micro-meterological phenomena, with particular emphasis on NO_x, which directly challenges the assumption that the air mass is homogeneously mixed. For the modeling of chain length, however, the imbalance does not present a fundamental limitation because our two chain length parameters are either only based on the production term (n(OH)), or on the branching ratio of radical loss versus propagation (ω). Neither chain length parameter convolutes radical initiation and termination processes.

4 Individual day modeling

The modeling results are quantified in terms of radical initiation, propagation, and termination routes for individual days for the i) HO_x-unconstrained (left) and ii) HO_x-constrained cases (right) in Table 2 - other parameters are also included, and are discussed in greater detail below. Note that the meteorology classification listed in the last row of each of the tables is taken from de Foy et al. (2005). In the event that the continuous collection of data was interrupted, the data gaps were filled by either a) extrapolating based on the median concentration profiles, or b) linearly correlated based on the final measurement before and the first measurement following the gap. Note the variability in radical initiation and cycling on different days. For instance, we report total RO_x radical initiation as low as 219 x 10^5 $\mathrm{molec.\ cm^{-3}\ s^{-1}}$ on 18/03 and as high as 808 x 10^5 $\mathrm{molec.\ cm^{-3}\ s^{-1}}$ on 15/03. Similarly, we observe the lowest rates of recycling on 18/03; however, we observe the highest rates of recycling on 23/03 because of comparable initiation coupled with higher NO concentrations as compared to 15/03.

5 VOC_R and NO_x

We use an ozone isopleth-type graph in Figure 3 to illustrate the relationship between P(O_3) and VOC_R and NO_x - these plots are similar to those shown in Kleinman et al. (2005). We observe very high values for both VOC_R and NO_x in Mexico City; much higher than in all US

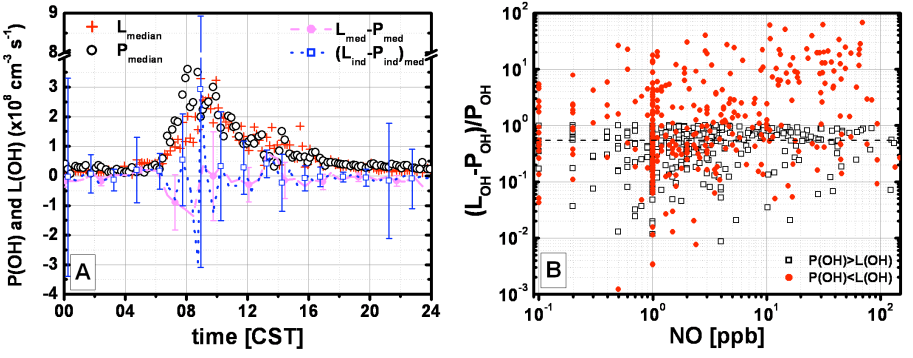

Fig. 2. A) Median OH production (open black circles) and loss (red plusses) are plotted against the difference between them with a 2σ experimental uncertainty, as replicated from Shirley et al. (2006) (closed magenta circles, dashed line). The median difference between individual experimentally determined P(OH) and L(OH) terms is shown (blue open square, dotted line) with a 2σ standard deviation. (Note the break in the y-scale between 4-7 x10^8 cm^{-3}s^{-1}; the error bars extend equally as far in the negative direction but are not shown). B) The difference in OH production and loss is shown in relative terms by dividing by production (and when values are negative, the absolute value was used). The values are separated by P(OH)>L(OH) (black squares) and P(OH)<L(OH) (red circles). In principle, the difference should be 0. The dotted line represents an inferred experimental uncertainty, meaning that all points *above* this line fall outside a 2σ experimental uncertainty and represent an imbalance in the measurements.

urban airmasses e.g., Houston, Nashville, New York, and Phoenix Kleinman et al. (2005). We observe a near-constant upward sloping relationship between $\mathrm{VOC_R}$ and $\mathrm{NO_x}$, indicating the colocation of VOC and $\mathrm{NO_x}$ sources.

The differences in measured and predicted $\mathrm{HO_x}$ radical concentrations yield different P($\mathrm{O_3}$) values, as shown in Figure 3-A and B. In panel B, there is a two-fold increase in the number of points with a predicted P($\mathrm{O_3}$) > 40 ppb hr^{-1} as compared to the $\mathrm{HO_x}$-unconstrained case.

Theory predicts that P($\mathrm{O_3}$) will reach a maximum at low $\mathrm{NO_x}$ concentrations and decreases

Table 2. Average reaction rates for RO_x radical pathways on individual days (in March) during MCMA-2003 from 07:00-13:00, as determined by a HO_x-unconstrained (left) and HO_x-constrained (right) model in units of 10^5 molec. cm^{-3} s^{-1}. Averaged values for measured HO_x concentrations (OH / HO_2), chain length (n(OH)), ozone production ($P(O_3)$), first order reactivity of OH and VOC (VOC-reac.), NO, $J(NO_2)$, and daily maxima of O_3, boundary layer height, CO are also shown to aid in the comparison of daily variations.

		9		**10**		**11**		**12**		**13**		**14**		**15**		**16**		**17**	
I1	OH initiation	139	140	284	284	232	233	193	193	252	253	147	147	323	324	244	243	265	266
T1	OH termination	232	216	370	371	273	385	211	241	247	219	198	206	365	286	330	376	354	317
I2	RO_2 initiation	82	80	171	172	120	178	108	129	144	142	89	93	166	150	152	167	153	147
T2	RO_2 termination	60	55	269	268	190	258	186	222	250	216	133	150	293	217	220	251	216	200
I3	RO initiation	6	4	8	8	13	15	5	6	8	7	4	4	9	8	9	10	9	8
T3	RO termination	20	18	33	33	22	34	20	26	24	24	18	18	37	32	33	38	31	29
I4	HO_2 initiation	102	100	262	263	181	289	150	173	195	193	134	137	260	242	234	249	228	221
T4	HO_2 termination	1	1	13	11	11	14	17	23	26	25	7	13	15	12	16	19	12	15
P1	$OH \rightarrow RO_2$	843	686	1445	1445	1345	1770	855	981	1284	1133	735	776	1503	1157	1265	1461	1308	1160
P2	$RO_2 \rightarrow RO$	755	620	1148	1152	1216	1585	690	788	1073	972	588	606	1170	938	1034	1191	1126	998
	via NO	505	432	840	835	855	1081	517	571	802	703	428	426	855	661	754	847	812	695
	via RO_2	236	176	293	294	376	475	173	202	271	250	160	169	315	259	280	321	313	285
P-2	$RO \rightarrow RO_2$	139	102	200	200	267	332	122	142	185	167	101	107	220	175	196	225	206	186
P3	$RO \rightarrow HO_2$	574	476	877	880	903	1190	525	600	817	741	450	463	886	709	777	896	854	756
P4	$HO_2 \rightarrow OH$	1047	2628	1750	2844	1553	5424	993	1735	1460	2322	893	1740	1796	2318	3691	3491	1587	2889
P5	$OH \rightarrow HO_2$	105	78	205	204	156	231	113	132	171	149	101	112	237	183	179	204	180	166
	chain length	2.8	9.2	2.6	5.0	3.0	8.8	2.5	4.2	2.8‘	4.2	2.6	4.9	2.6	3.9	2.6	5.9	2.6	4.5
	$P(O_3)$ (ppb/hr)	27.2	54.0	42.3	62.5	40.0	115.1	24.1	38.5	37.3	52.2	21.2	36.8	42.7	50.5	37.3	78.8	39.0	61.9
	OH / HO_2 (ppt)	0.08 / 3.0		0.20 / 8.7		0.20 / 11.5		0.23 / 14.0		0.23 / 15.7		0.21 / 11.7		0.20 / 11.5		0.22 / 13.9		0.21 / 12.4	
	O_3max (ppb)	130		146		78		150		109		144		156		156		115	
	VOC-reactivity (s^{-1})	49		50		67		37		43		28		35		52		42	
	NO (ppb)	37		36		54		15		16		17		17		37		26	
	$J(NO_2)$ (x10^{-3} s^{-1})	2.7		5.5		5.4		6.7		6.5		5.8		6.1		6.0		6.3	
	PBL (km)	1.9		1.9		2.3		–		3.3		2.9		3.5		3.5		3.3	
	COmax (ppm)	4.2		5.2		8.5		4.2		4.0		2.8		2.5		4.7		3.4	
	meteorology	cold surge		cold surge		cold surge		O3-North		O3-North		O3-South		O3-South		O3-South		O3-South	

at higher NO_x concentrations: We observe this in the HO_x-unconstrained case, however, we do not observe this to be true in the HO_x-constrained case. The VOC loadings in Mexico City are sufficiently high at high NO_x concentrations as to perpetuate radical cycling, rather than allowing the termination pathways via NO_x reactions to dominate. The measured HO_x concentrations at concurrently high VOC and NO_x loadings characterize a previously unidentified scenario for ozone production rates.

Kleinman et al. (2005) also employ a novel parameter L_N/Q to understand the VOC and

		18		19		20		21		22		23		24		25		26	
I1	OH initiation	84	84	211	212	222	223	262	263	252	254	278	278	205	206	211	212	183	183
T1	OH termination	79	52	226	200	216	191	253	243	221	143	298	250	161	139	278	286	233	216
I2	RO_2 initiation	54	48	149	146	144	142	156	155	159	132	210	199	98	99	145	155	153	156
T2	RO_2 termination	79	62	238	203	240	195	272	236	302	182	343	272	187	131	221	203	227	196
I3	RO initiation	2	1	6	5	7	6	7	6	7	4	9	7	4	3	7	7	7	6
T3	RO termination	10	7	25	23	23	22	29	29	27	20	40	37	19	18	30	33	29	30
I4	HO_2 initiation	81	73	215	211	213	210	237	235	231	200	319	306	156	153	242	252	245	248
T4	HO_2 termination	29	28	36	35	48	33	52	35	46	20	68	41	51	31	31	29	51	39
P1	$OH \rightarrow RO_2$	522	336	1255	1101	1231	1062	1272	1168	1337	840	1575	1310	844	661	1164	1160	1066	972
P2	$RO_2 \rightarrow RO$	419	276	1027	928	1011	913	1009	959	1061	717	1256	1096	669	573	963	999	881	840
	via NO	273	175	744	648	727	634	744	685	766	495	923	778	475	394	710	717	642	592
	via RO_2	146	96	283	262	284	262	265	255	295	209	333	297	194	168	253	263	239	232
P-2	$RO \rightarrow RO_2$	72	49	168	150	178	159	175	165	181	120	223	191	122	100	172	173	164	152
P3	$RO \rightarrow HO_2$	330	215	791	715	771	698	771	733	815	550	962	840	511	439	730	759	666	637
P4	$HO_2 \rightarrow OH$	620	791	1476	1940	1434	1954	1490	2257	1517	1177	1864	2979	970	1768	1426	3719	1303	2638
P5	$OH \rightarrow HO_2$	96	62	195	170	198	167	215	193	199	126	255	208	161	112	185	173	177	154
	chain length	3.1	4.3	3.0	4.4	2.8	4.1	2.7	5.4	2.9	3.0	2.8	5.4	2.5	5.2	2.7	6.9	2.6	5.7
	$P(O_3)$ (ppb/hr)	15	17	37	45	36	45	37	51	38	29	47	66	24	38	35	78	32	57
	OH / HO_2 (ppt)	0.22 / 20.1		0.24 / 18.2		0.23 / 18.4		0.22 / 15.6		0.16 / 12.0		0.20 / 16.1		0.21 / 16.8		0.20 / 18.8		0.18 / 19.0	
	O_{3max} (ppb)	77		135		117		136		147		58		132		122		121	
	VOC-reactivity (s^{-1})	13		35		32		36		35		49		29		45		38	
	NO (ppb)	4		13		12		20		13		28		20		28		16	
	$J(NO_2)$ (x10^{-3} s^{-1})	6.2		6.0		6.2		5.8		5.8		6.8		6.8		6.8		6.8	
	PBL (km)	3.1		1.5		2.5		2.9		1.5		–		3.5		3.5		3.0	
	CO_{max} (ppm)	1.6		2.8		2.4		3.9		1.9		4.6		3.8		5.8		4.3	
	meteorology	O3-North		cold surge		cold surge		cold surge		cold surge		O3-North		O3-North		O3-North		O3-North	

NO_x limitations of ozone production, where L_N is the sum of RO_x radical loss rates due to reaction with NO_x and Q is the summation of new radical production. While our explicit model is ideally suited to predict this parameter, and compare to values presented by Kleinman et al. (2005), the HO_x-constrained code presents a problem because it is unbalanced with regard to radical production and destruction. This imbalance results in higher than expected values for L_N, resulting in values for the L_N/Q parameter well above 1. These values do not make physical sense, and as such, we are unable to use the L_N/Q parameter in the same manner as Kleinman et al. (2005) to draw conclusions about the VOC and/or NO_x sensitivity of the MCMA.

Our near-explicit code does, however, provide the means to test some of the basic assumptions employed to derive the L_N/Q parameter to the MCMA. The approximation of L_N being equivalent to the flux from the reaction of OH with NO_2 i.e., that the formation of organic nitrates via reaction of RO_2 with NO is negligible, under-estimates L_N by some 15-30% throughout the day. In determining the relationship between L_N/Q relative to VOC reactivity and NO_x reactivity, Kleinman et al. (2001) also make the following assumption. In the limit that chain

propagation is much more important than chain initiation and termination:

$$k_{OH+VOC}[OH][[VOC]=k_{HO_2+NO}[HO_2][[NO] \quad (3)$$

Even though the VOC loadings are high and radical cycling is fast in the MCMA, this assumption breaks down in the high NO_x environment in the MCMA. Based on our model, by not accounting for other radical pathways i.e., $OH \rightarrow HO_2$ (P5 in Figure 1) or OH termination (T1 in Figure 1) in their approximation, Kleinman et al. (2001) introduce an uncertainty of about 20%. In the HO_x-constrained model, the measured concentrations of HO_2 are higher than in the unconstrained case, and the radical flux of $HO_2 \rightarrow OH$ is subsequently much higher than OH loss via reaction with VOC. As such, the assumption by Kleinman et al. (2001) introduces a minimum uncertainty of 20%, and a maximum of a factor of 5 (i.e., 500%) in the HO_x-constrained case. Combining the uncertainty in the determination of L_N and the imbalance in the assumption relative to OH production and loss, we estimate a lower-limit of uncertainty in the L_N/Q parameter of some 30%. Furthermore, this does not account for any uncertainty in the Q parameter; depending on the time of day, O_3 and HCHO photolysis and O_3/alkene reactions account for 29-65% of the value of Q (Volkamer et al., 2010). The traditional definition of Q accounts for O_3 and HCHO photoysis; based on results from Volkamer et al. (2010) these in sum account for less than half of the radical initiation in the MCMA. We also note that the quantitative use of the L_N/Q parameter requires accounting for an expanded radical initiation scheme that also accounts for the other radical sources. Despite these limitations, an expanded L_N/Q concept can conceivably applied to the MCMA.

In the lower panel of Figure 3, the shapes on the graph indicate the VOC_R and NO_x 'coordinates' of $P(O_3)$ values reported in a 5-city study by Kleinman et al. (2005), with the range of $P(O_3)$ generally between 20-60 $ppb\ hr^{-1}$. The higher ozone production rates reported for the MCMA are consistent with the higher VOC loadings and the high NO_x environment. Even though NO_x levels in the MCMA are up to an order of magnitude higher than other urban areas, the ozone production levels do not scale linearly because of the increased radical flux along loss routes for OH and RO_2 with NO_2 and NO, respectively. It is also worth noting that we consider our values for $P(O_3)$ as an under-estimate based on lower-than-expected RO_2 values. In other

urban studies, as indicated by the dark and light gray shaded lines in Figure 5-B they note a RO_2-to-HO_2 ratio of roughly 1, whereas a HO_x-constrained calculation here indicates a much lower value (0.2); a RO_2-to-HO_2 value of 0.8, for instance, may result in ozone production levels about 40-50 $\mathrm{ppb\ hr^{-1}}$ higher.

References

Axelsson, H., Eilard, a., Emanuelsson, a., Galle, B., Edner, H., Ragnarson, P., and Kloo, H.: Measurement of Aromatic-Hydrocarbons with the Doas Technique, Applied Spectroscopy, 49, 1254–1260, 1995.

de Foy, B., Caetano, E., Magana, V., Zitacuaro, A., Cardenas, B., Retama, A., Molina, L., and Molina, M.: Mexico City basin wind circulation during the MCMA-2003 field campaign, Atmospheric Chemistry and Physics, 5, 2267–2288, 2005.

EPA: Hazardous Air Pollutants: EPA AirData Monitor Values Report, Tech. rep., US Environmental Protection Agency, http://www.epa.gov/air/data, 2004.

Harley, R. A., Hannigan, M. P., and Cass, G. R.: Respeciation of Organic Gas Emissions and the Detection of Excess Unburned Gasoline in the Atmosphere, Environmental Science and Technology, 26, 2395–2408, 1992.

Kleinman, L. I., Daum, P. H., Lee, Y. N., Nunnermacker, L. J., Springston, S. R., Weinstein-Lloyd, J., and Rudolph, J.: Sensitivity of ozone production rate to ozone precursors, Geophysical Research Letters, 28, 2903–2906, 2001.

Kleinman, L. I., Daum, P. H., Lee, Y. N., Nunnermacker, L. J., Springston, S. R., Weinstein-Lloyd, J., and Rudolph, J.: A comparative study of ozone production in five U.S. metropolitan areas, Journal of Geophysical Research-Atmospheres, 110, D02 301, 2005.

Shirley, T. R., Brune, W. H., Ren, X., Mao, J., Lesher, R., Cardenas, B., Volkamer, R., Molina, L. T., Molina, M. J., Lamb, B., Velasco, E., Jobson, T., and Alexander, M.: Atmospheric oxidation in the Mexico City Metropolitan Area (MCMA) during April 2003, Atmospheric Chemistry and Physics, 6, 2753–2765, 2006.

Velasco, E., Lamb, B., Westberg, H., Allwine, E., Sosa, G., Arriaga-Colina, J. L., Jobson, B. T., Alexander, M., Prazeller, P., Knighton, W. B., Rogers, T. M., Grutter, M., Herndon, S. C., Kolb, C. E., Zavala, M., de Foy, B., Volkamer, R., Molina, L. T., and Molina, M. J.: Distribution, magnitudes, reactivities,

ratios and diurnal patterns of volatile organic compounds in the Valley of Mexico during the MCMA 2002 & 2003 field campaigns, Atmospheric Chemistry And Physics, 7, 329–353, 2007.

Volkamer, R., Etzkorn, T., Geyer, A., and Platt, U.: Correction of the oxygen interference with UV spectroscopic (DOAS) measurements of monocyclic aromatic hydrocarbons in the atmosphere, Atmospheric Environment, 32, 3731–3747, 1998.

Volkamer, R., Molina, L. T., Molina, M. J., Flores, E., Grutter, M., Galle, B., Mellqvist, J., Samuelsson, J., Knighton, B., and Jobson, B. T.: Open-path Emission Factors Derived from DOAS and FTIR Measurements in the Mexico City Metropolitan Area, American Geophysical Union, Fall Meeting Supplement, 85, Abstract A11A–0003, 2004.

Volkamer, R., Molina, L., Molina, M., Shirley, T., and Brune, W. H.: DOAS measurement of glyoxal as an indicator for fast VOC chemistry in urban air, Geophysical Research Letters, 32, L08 806, 2005.

Volkamer, R., Jimenez, J. L., San Martini, F., Dzepina, K., Zhang, Q., Salcedo, D., Molina, L. T., Worsnop, D. R., and Molina, M. J.: Secondary organic aerosol formation from anthropogenic air pollution: Rapid and higher than expected, Geophysical Research Letters, 33, 4, 2006.

Volkamer, R., Sheehy, P., Molina, L., and Molina, M.: Oxidative capacity of the Mexico City atmosphere - Part 1: A radical source perspective, Atmospheric Chemistry and Physics, 2010.

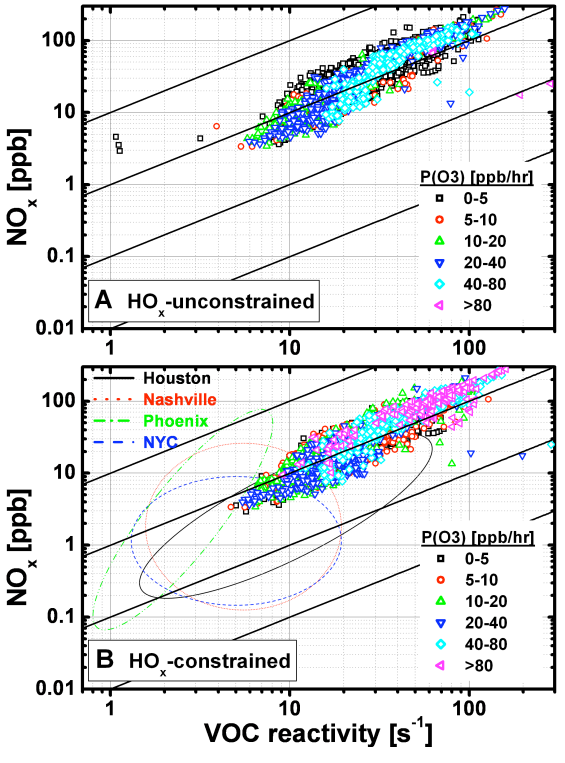

Fig. 3. Ozone production rates shown are shown as a function of $\mathrm{VOC_R}$ and $\mathrm{NO_x}$ in the $\mathrm{HO_x}$-unconstrained (A) and $\mathrm{HO_x}$-constrained cases (B). Note the increased prevalence of higher $\mathrm{P(O_3)}$ values in panel B (80+ $\mathrm{ppb\ hr^{-1}}$), as represented by the magenta left-triangles. Panel B also shows traces of ozone production rates as determined for other cities (Kleinman et al., 2005): Houston (black, solid line), Nashville (red, dotted line), Phoenix (green, dash-dot line), and New York City (blue, dashed line). The diagonal isolines represent constant $\mathrm{VOC_R/NO_x}$ ratios.